Cancer Research

Astrocytes Promote Medulloblastoma Progression through Hedgehog Secretion

Yongqiang Liu[1], Larra W. Yuelling[1], Yuan Wang[2], Fang Du[1], Renata E. Gordon[1], Jenny A. O'Brien[1], Jessica M.Y. Ng[3], Shannon Robins[1], Eric H. Lee[1], Hailong Liu[1], Tom Curran[3], and Zeng-Jie Yang[1,2]

Abstract

Astrocytes, the most abundant type of glial cells in the brain, play critical roles in supporting neuronal development and brain function. Although astrocytes have been frequently detected in brain tumors, including medulloblastoma (MB), their functions in tumorigenesis are not clear. Here, we demonstrate that astrocytes are essential components of the MB tumor microenvironment. Tumor-associated astrocytes (TAA) secrete the ligand sonic hedgehog (Shh), which is required for maintaining MB cell proliferation despite the absence of its primary receptor Patched-1 (Ptch1). Shh drives expression of Nestin in MB cells through a smoothened-dependent, but Gli1-independent mechanism. Ablation of TAA dramatically suppresses Nestin expression and blocks tumor growth. These findings demonstrate an indispensable role for astrocytes in MB tumorigenesis and reveal a novel Ptch1-independent Shh pathway involved in MB progression. *Cancer Res; 77(23); 6692–703. ©2017 AACR.*

Introduction

Astrocytes are specialized glial cells, distributed ubiquitously throughout the brain, that play essential roles in microcirculation, provision of energy metabolites to neurons, and homeostasis maintenance of extracellular ions and neurotransmitters (1, 2). Antibodies against glial fibrillary acid protein (GFAP) are often used to detect astrocytes (3), sometimes in conjunction with antibodies specific for other biomarkers such as S100β (4), astrocyte cell surface antigen 2 (ACSA-2; ref. 5), and brain lipid binding protein (BLBP; ref. 6) in immunohistochemistry assays. Astrocytes in the cerebellum, often referred to as Bergmann glial cells, provide critical functions that support proliferation and migration of cerebellar granule neuron precursors (GNP; ref. 7). Under pathological brain conditions, such as trauma or malignant growth, astrocytes undergo astrogliosis, upregulating GFAP expression, increasing proliferation, and enduring pronounced hypotrophy (8, 9). This process has been linked to elevated expression of survival genes in tumor cells that have been proposed to provide protection from chemotherapeutic agents (10). In addition, astrocytes release numerous growth factors and cytokines that potentially provide a supportive microenvironment for brain tumor growth and metastasis.

Medulloblastoma (MB) is the most common malignant brain tumor in children. Approximately 30% of human MBs result from aberrant activation of the hedgehog signaling pathway (11–13). The hedgehog pathway plays fundamental roles during normal development by regulating multiple processes involved in tissue patterning, proliferation, and differentiation (14). Three mammalian hedgehog homologues, Sonic hedgehog (Shh), Indian hedgehog, and Desert hedgehog, activate the hedgehog pathway by binding to and inhibiting the receptor Patched-1 (Ptch1). This relieves the inhibitory effect of Ptch1 on Smoothened (Smo), which then translocates to the primary cilium in an active form. Activated Smo then suppresses the function of suppressor-of-fused (Sufu), allowing Gli1 and Gli2 to translocate to the nucleus and increase transcription of a set of target genes, including *Ptch1* and *Gli1*. Gli3, an additional Gli family member that is positively regulated by Sufu, predominately serves as a negative regulator of hedgehog signaling (15, 16). Elevated expression of Gli1 is a hallmark of hedgehog pathway activation. However, substantial evidence indicated that not all hedgehog activity requires Gli1 (17, 18). Shh has been shown to induce cytoskeletal rearrangements in mouse fibroblasts independently of Gli1 (19). Furthermore, activation of Src family kinases by Shh in commissural neurons, occurs via a Gli1-independent mechanism (20).

Previously, we showed that deletion of *Ptch1* in mouse cerebellar GNPs results in MB formation with 100% penetrance confirming GNPs as the cell of origin for hedgehog group MB (21). However, after a prolonged period of proliferation, the majority of GNPs ultimately differentiated, despite the loss of *Ptch1*. Only a small subset of *Ptch1*-deficient GNPs developed into tumors, suggesting that although loss of *Ptch1* alone is necessary for tumor formation, it is not sufficient for malignant transformation of cerebellar GNPs (21). Recently, we reported that expression of Nestin, a type VI intermediate filament protein, is required for *Ptch1*-deficient GNPs to form MB. Nestin augmented

[1]Cancer Biology Program, Fox Chase Cancer Center, Temple University Health System, Philadelphia, Pennsylvania. [2]Laboratory of Molecular Neuropathology, College of Pharmaceutical Sciences, Soochow University, Suzhou, Jiangsu, China. [3]Children's Research Institute, Children's Mercy Kansas City, Kansas City, Missouri.

Note: Supplementary data for this article are available at Cancer Research Online (http://cancerres.aacrjournals.org/).

Y. Liu and L.W. Yuelling contributed equally to this article.

Corresponding Author: Zeng-jie Yang, Fox Chase Cancer Center, 333 Cottman Avenue, Philadelphia, PA 19111. Phone: 215-214-1545; Fax: 919-451-8071; E-mail: zengjie.yang@fccc.edu

doi: 10.1158/0008-5472.CAN-17-1463

hedgehog pathway activity by binding to Gli3, thereby abolishing its inhibitory function (22). These data reveal that Nestin expression is indispensable for MB tumorigenesis. However, the mechanism underlying Nestin expression in MB cells has not been identified.

Here, we demonstrate that astrocytes, enriched in both human and mouse MB tissue, represent a key functional component of the tumor microenvironment. Tumor-associated astrocytes (TAA) were found to express and secrete Shh to promote MB cell proliferation. Astrocyte-derived Shh induced Nestin expression in MB cells through a Smo-dependent, but Gli1-independent mechanism. Genetic ablation of TAA dramatically inhibited Nestin expression in MB cells, resulting in reduced proliferation and a block in tumor growth. Thus, astrocytes play a critical role in supporting MB growth by secreting the mitogen Shh into the tumor microenvironment.

Materials and Methods

Mice

Ptch1$^{fl/fl}$ mice, *Nestin-CFP* mice have been described previously (22). *Math1-Cre* Mice, *Ptch1-lacZ* mice, *GFAP-GFP* mice, *GFAP-TK* mice, and *Rosa26-SmoM2* mice were from Jackson Labs. All animals were maintained in the LAF at Fox Chase Cancer Center and all experiments were performed in accordance with procedures approved by the Fox Chase Cancer Center Animal Care and Use Committee.

Cell isolation, flow cytometry, and cell culture

GNPs were isolated from cerebella of P4-P7 mice, and MB cells from adult cerebella as previously described (23). Briefly, Cerebella were digested in a solution containing 10 U/mL papain (Worthington), 200 μg/mL L-cysteine (Sigma), and 250 U/mL DNase (Sigma) to obtain a single cell suspension, and then centrifuged through a 35% to 65% Percoll gradient (Sigma). Cells from the 35% to 65% interface were suspended in NB-B27 (Neurobasal with B27 supplement, 1 mmol/L sodium pyruvate, 2 mmol/L L-glutamine, and Pen/Strep, all from Invitrogen). CFP-negative GNPs from p4 *Math1-Cre/Ptch1*$^{fl/fl}$*/Nestin-CFP* cerebella were then purified using a FACS Aria II (BD Bioscience). GNPs and MB cells were suspended in NB-B27 and plated on poly-D-lysine (PDL)-coated 24-well plates for further experiments.

Histology, IHC, and Western blotting

Primary antibodies used in this study include: anti-Nestin (1:1,000; Abcam), anti-GFAP (1:500; BD), anti-S100 (1:500; Sigma), anti-BLBP (1:500; Millipore), anti-Ki67 (1:500; BD), anti-NeuN (1:200; millipore), anti-GFP (1:500; Millipore), anti-Cre (1:500; Novagen), anti-BrdUrd (1:500; Sigma), anti-Shh (1:500; BD), anti-Gli1 (1:1000; CST), anti-GAPDH (1:2000; Sigma), and anti-HA (1:200; Covance). Secondary antibodies include: Alexa Fluor 594 anti-rabbit IgG (1:200), Alexa Fluor 594 anti-mouse IgG (1:200), Alexa Fluor 594 anti-chicken IgY (1:200), Fluor 488 anti-rabbit IgG (1:200), Fluor 488 anti-mouse IgG (1:200), Fluor 488 anti-chicken IgY (1:200) from Invitrogen.

For immunohistochemistry, mice were perfused with PBS followed by 4% paraformaldehyde (PFA). Cerebella were removed and fixed overnight in 4% PFA, cryoprotected in 30% sucrose, frozen in Tissue Tek-OCT (Sakura Finetek) and cut into 10 to 12 μm sagittal sections. Immunofluorescent staining for sections and cultured cells was carried out according to standard protocols. Briefly, after fixation in 4% PFA, sections or cells were blocked and permeabilized for 1 hour with PBS containing 0.1% Triton X-100 and 10% normal goat serum, stained with primary antibodies overnight at 4°C, and incubated with secondary antibodies for 2 hours at room temperature. Sections were counterstained with DAPI and mounted with Fluoromount G (Southern Biotechnology) before being visualized using a Nikon Eclipse Ti microscope.

For Western blot analysis, cells were lysed in RIPA buffer (Thermo Scientific) supplemented with protease and phosphatase inhibitors. Total lysate containing equal amount of protein were separated by SDS-PAGE gel and subsequently transferred onto PVDF membrane. Membranes were then subjected to probe with antibodies. Western blot signals were detected by using SuperSignal West Pico Chemiluminescent substrate (Thermo Scientific).

Astrocytes isolation and culture

TAAs were isolated from MB tissues from *Math1-Cre/Ptch1*$^{fl/fl}$*/GFAP-GFP* mice at 8 weeks of age. Briefly, MB tissues were digested using papain dissociation system to obtain a single cell suspension as mentioned above, the cells were suspended in DPBS plus 0.5% BSA, and stained with anti-ACSA-2-APC (1:500; Miltenyi Biotec), TAA were collected by harvesting GFP$^+$/ACSA2-APC$^+$ cells using FACS. For coculture of TAA with GNPs and MB cells, isolated TAA were cultured in PDL-coated wells for 3 days, then purified GNPs or MB cells were added on top of TAA at a ratio of 5 to 1, and cocultured for indicated time period.

For detection of Shh ligand by ELISA assay, the culture medium (CM) for astrocytes was replaced with serum-free DMEM medium after being cultured with serum for 3 days. Conditioned CM was harvested 2 days later, the concentration of Shh ligand was measured using the mouse Shh-N ELISA Kit (Sigma).

For luciferase assay, shh-light II cells (ATCC CRL-2795) were cultured in DMEM with 10% FBS. After the cells reached 70% to 80% confluence, the medium was replaced with DMEM without FBS (naïve CM), 50% Shh-CM or TAA-CM for 2 days, then luciferase levels in shh-light II cells were measured using Dual-Luciferase Reporter Assay (Promega).

MRI

MR microimaging was performed using intense magnetic fields on a 7 Tesla wide bore system (ESPREE) according to the standard protocol. MRI image analysis and tumor volume calculation was performed using Image J software (version 1.46; NIH, Bethesda, MD), which has Bruker plugins that can read reconstructed date files (2dseq) from Bruker Biospec spectrometer. The regions of interest were drawn manually covering the entire tumor area on each slice of the MRI images, and the areas of the individual slices were summed afterwards. The tumor volume was calculated by multiplying summated areas by slice thickness.

Slice culture

Cerebella were harvested from *Math1-Cre/Ptch1*$^{fl/fl}$*/Nestin-CFP* mice. A total of 250 μm slices were prepared using a VT1000S vibratome (Leica Microsystems) as previously described (24). Tumor tissue slices were transferred onto a Millicell cell culture membrane inserts (0.4 μm, 30-mm diameter; Merck Millipore) in a 6-well plate with 1-mL DMEM CM containing 25 mmol/L HEPES. Tumor tissue slices receives medium from below and air

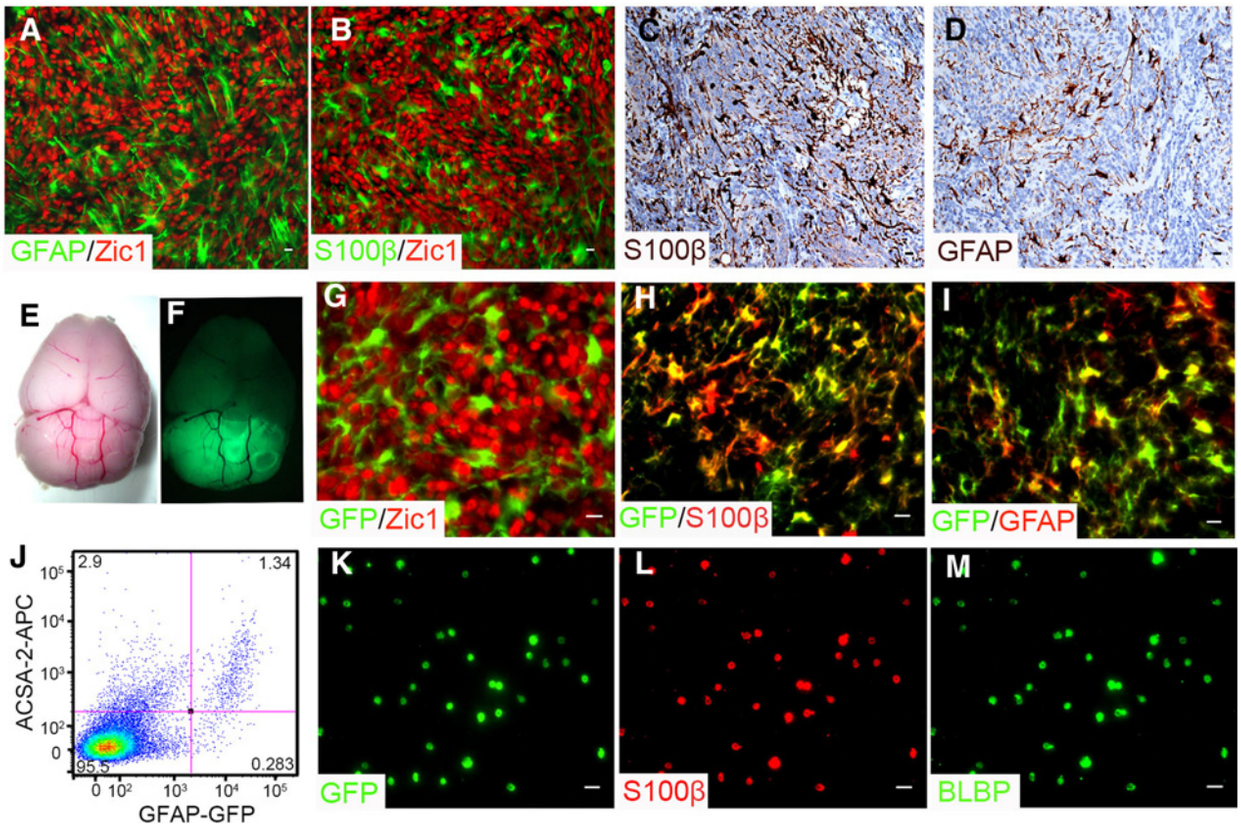

Figure 1.

Astrocytes are enriched in Shh type MB. **A** and **B,** Sagittal sections from *Math1-Cre/Ptch1*$^{fl/fl}$ cerebella at 8 weeks of age were immunostained for GFAP and Zic1 (**A**) or S100β and Zic1 (**B**). **C** and **D,** Astrocytes in human MBs were examined by immunohistochemistry for S100β (**C**) and GFAP (**D**). **E** and **F,** Whole-mount images of mouse brain from a *Math1-Cre/Ptch1*$^{fl/fl}$*/GFAP-GFP* mouse at 8 weeks of age in bright field (**E**) and GFP channel (**F**). **G–I,** Sagittal sections from *Math1-Cre/Ptch1*$^{fl/fl}$*/GFAP-GFP* cerebella were immunostained for GFP and Zic1 (**G**), GFP and S100β (**H**), or GFP and GFAP (**I**). **J,** Cells harvested from *Math1-Cre/Ptch1*$^{fl/fl}$*/GFAP-GFP* cerebella at 8 weeks of age were stained for ACSA2, and analyzed for ACSA2 (APC) and GFAP (GFP) expression by flow cytometry. **K–M,** Purified TAAs were immunostained for GFP (**K**), S100β (**L**), and BLBP (**M**) at 0 hr (right after being plated). Scale bar, 10 μm.

from above, and were cultured in an incubator with 5% CO_2 at 37°C for indicated times.

RT-PCR

RNA was extracted from GNPs or MB cells using RNeasy Mini Kit (Qiagen). For real-time PCR, first-strand cDNA was synthesized from equal amounts of RNA using Superscript III Reverse Transcriptase (Invitrogen). Triplicate reactions were prepared using TaqMan probe real-time PCR, and real-time quantification was performed on a BIORAD iCycler iQ system (Bio-Rad). Primer sequences are available upon request.

In situ hybridization

Tumor-bearing mice were perfused with 4% PFA; brains were embedded in OCT and cut into 12-μm sections. Sections were fixed in 4% PFA, acetylated and incubated for 1 hour at room temperature in prehybridization buffer (50% formamide, 5X SSC, 1X Denhardt's solution, 10% dextran sulfate, 1 mg/mL yeast tRNA, 40 μg/mL salmon sperm DNA). Digoxigenin (DIG)-UTP–labeled probes for Shh were denatured and added to this mix on the section, and hybridization was performed at 59°C for 40 hours. Probes were synthesized using a DIG Labeling Kit (Roche). After hybridization, sections were incubated overnight at 4°C with alkaline phosphatase–conjugated anti-DIG antibodies (Roche). Bound probe was visualized by incubating sections in NBT/BCIP (Roche) overnight in the dark. Coverslips were mounted with Aqua-Polymount (Polysciences).

Statistical analysis

Unpaired *t* test was performed to determine the statistical significance of the difference. $P < 0.05$ was considered statistically significant. Error bars, SEM. Data handling and statistical processing were performed using GraphPad Prism Software.

Results

Astrocytes are enriched in MB tissue

Human MB comprises at least four subgroups: Wnt, Shh, group 3, and group 4, with the Shh group accounting for approximately 30% of cases (11, 25, 26). Conditional genomic deletion of *ptch1* in cerebellar GNPs led to MB formation in *Math1-Cre/Ptch1*$^{fl/fl}$ mice (21). We examined the presence of astrocytes in MB tissues from *Math1-Cre/Ptch1*$^{fl/fl}$ mice by IHC. As shown in Fig. 1A and B, a significant number of TAA (GFAP$^+$ or S100β$^+$) were identified,

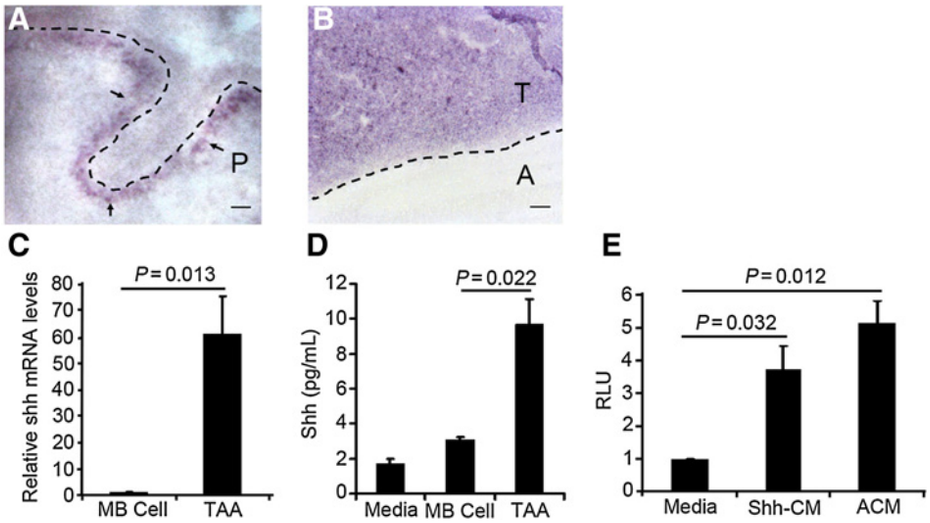

Figure 2.

TAAs secrete Shh. **A** and **B,** Sagittal sections from wild-type cerebella at P8 (**A**) and MB (**B**) were examined for Shh mRNA expression by *in situ* hybridization. Note that Shh mRNA was found in the purkinje cell layer of the wild-type cerebellum (**A**) and MB tissue (**B**). P, Purkinje cell layer; T, tumor tissue; A, adjacent normal cerebellum. The dotted line in **A** indicates the molecular layer of wild-type cerebellum. **C,** Expression of *Shh* mRNA in MB cells and TAAs was examined by qPCR. **D,** Concentrations of Shh ligand in conditioned culture media collected from control (naïve CM), MB cell culture, or TAA culture were measured by an ELISA kit. **E,** Relative luciferase level (RLU) in Shh-light II cells cultured with recombinant Shh (Shh-CM) or TAA-conditioned CM (ACM) for 2 days. The values in **C**, **D**, and **E** are the means ± SEM from three independent experiments. Scale bar, 20 μm.

intermingled with MB cells ($Zic1^+$; ref. 27) throughout the tumor mass. Similarly, astrocytes were also detected in human Shh type MB tissue (Fig. 1C and D) as well as in MBs derived from *Ptch1* heterozygous mice (28) and mice carrying constitutively activated Smo in cerebellar GNPs (Supplementary Fig. S1A–S1D; ref. 29). These data suggest that astrocytes are abundant in the MB tumor microenvironment.

To investigate the possible role of astrocytes in MB tumorigenesis, we purified TAA from *Math1-Cre/Ptch1$^{fl/fl}$* mice that had been crossed with *GFAP-GFP* mice that express GFP in astrocytes (30). We observed a robust GFP signal in MBs arising in *Math1-Cre/Ptch1$^{fl/fl}$/GFAP-GFP* mice at 8 weeks of age (Fig. 1E and F), but there were no MB cells ($Zic1^+$) positive for GFP (Fig. 1G). In contrast, the majority of GFP^+ cells expressed the astrocyte makers, S100β (Fig. 1H) and GFAP (Fig. 1I). On the basis of flow cytometry analyses, 1% to 2% of cells dissociated from MB tissue in *Math1-Cre/Ptch1$^{fl/fl}$/GFAP-GFP* mice were positive for GFP. Approximately, 80% to 85% of the GFP^+ cells also expressed ACSA2 (Fig. 1J), a cell surface marker for astrocytes (31). Purified $GFP^+/ACSA2^+$ cells exclusively expressed S100β and BLBP (Fig. 1K–M), and no $Zic1^+$ were detected in the GFP+ population (data not shown). When cultured, purified $GFP^+/ACSA2^+$ cells solely gave rise to astrocytes based on marker expression and star-like morphology (Supplementary Fig. S1E–S1G). These data suggest that TAAs in MB tissue from *Math1-Cre/Ptch1$^{fl/fl}$/GFAP-GFP* mice represent $GFP^+/ACSA2^+$ cells. Therefore, for the following experiments, TAA were harvested by FACS purifying $GFP^+/ACSA2^+$ cells from MBs of *Math1-Cre/Ptch1$^{fl/fl}$/GFAP-GFP* mice.

TAA in MB tissue secrete Shh ligand

Previously, astrocytes in the cortex were reported to secrete Shh to support brain development (32). Therefore, we looked for the presence of Shh mRNA in MB tissue by *in situ* hybridization. At postnatal day 8 (P8), Shh mRNA was detected in the Purkinje layer of the cerebellum (Fig. 2A), consistent with previous reports demonstrating that Purkinje neurons secrete Shh to promote GNPs proliferation in neonatal mice (33). Abundant expression of Shh mRNA was found in MB tissue from *Math1-Cre/Ptch1$^{fl/fl}$* mice at 8 weeks of age (Fig. 2B), but not in adjacent normal tissue, suggesting that Shh-expressing cells exist in the MB microenvironment. To investigate whether *Shh* transcripts in the MB microenvironment are derived from astrocytes, we isolated TAA and MB cells from *Math1-Cre/Ptch1$^{fl/fl}$/GFAP-GFP* mice and examined Shh mRNA expression by qPCR. As shown in Fig. 2C, elevated levels of Shh mRNA expression were detected in TAA compared with MB cells, indicating that TAAs highly expressed Shh mRNA. Having observed increased expression of Shh mRNA in TAAs, we then tested whether TAA secreted Shh. MB cells and TAA isolated from *Math1-Cre/Ptch1$^{fl/fl}$/GFAP-GFP* mice were cultured *in vitro* for 3 days. Conditioned CM was collected to examine the presence of Shh by ELISA, and regular CM was used as a negative control. As shown in Fig. 2D, markedly increased levels of Shh ligand were detected in TAA-CM, compared to MB cell CM and regular culture medium. These data indicate that TAA, but not MB cells, secrete Shh in culture.

To determine whether TAA-derived Shh is functional, we investigated activation of the Shh pathway by TAA-CM in Shh-light II cells (34). TAA-CM was prepared as mentioned above, and Shh-light II cells were treated with TAA-CM or naïve CM with and without recombinant Shh as controls. As expected, the luciferase level was significantly elevated in Shh-light II cells treated with recombinant Shh, compared to treatment with control CM (Fig. 2E). Enhanced luciferase levels were also observed in Shh-light II cells after treatment with TAA-CM, suggesting that TAA-derived Shh markedly stimulated the hedgehog pathway in Shh-light II cells. Taken together, the

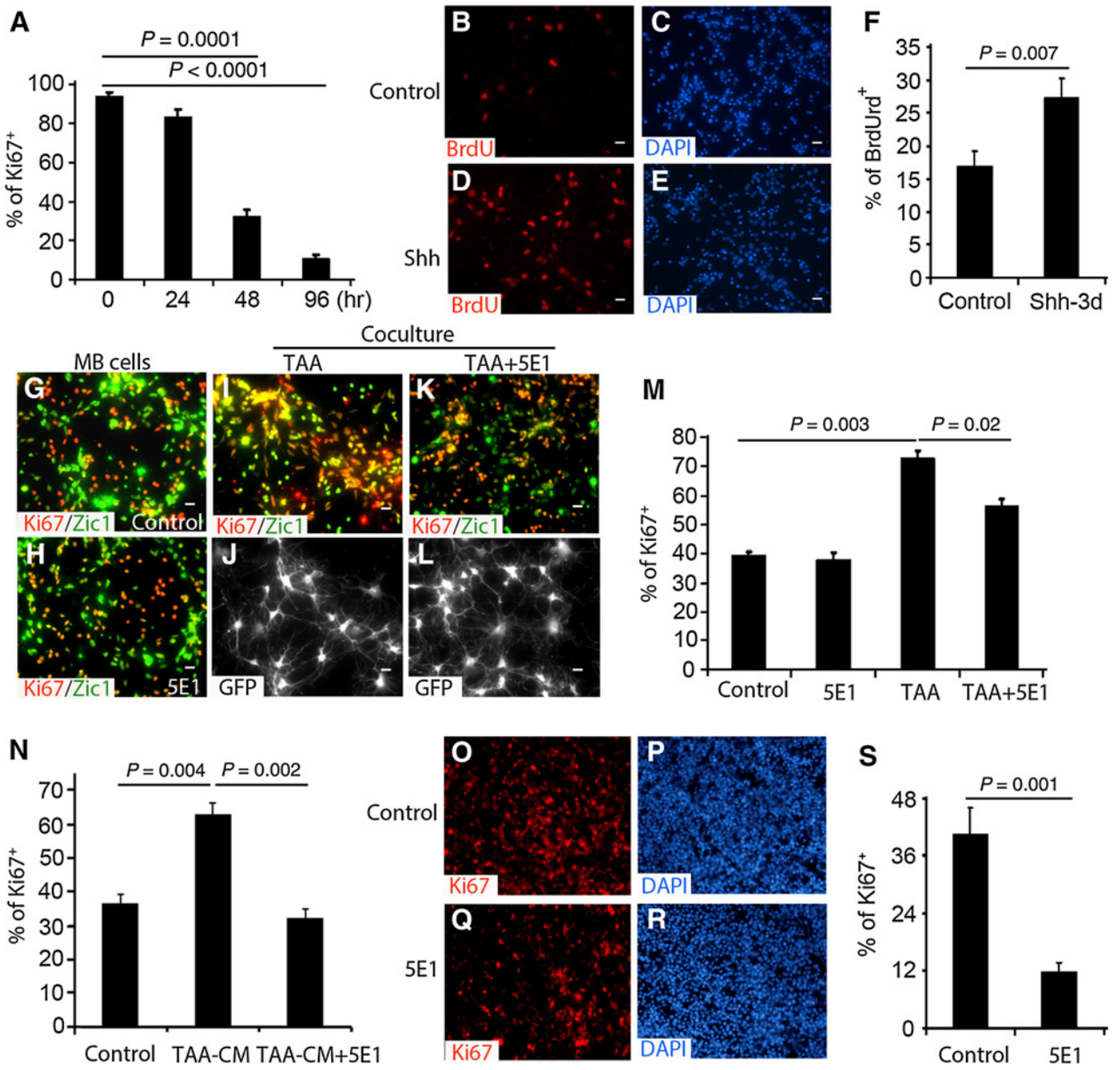

Figure 3.

TAA-derived Shh supports MB cell proliferation. **A,** Percentage of Ki67$^+$ cells among cultured MB cells harvested at designated time points (0–96 hours) was quantified. **B–E**, MB cells were treated with PBS control (**B** and **C**) or Shh (**D** and **E**) for 3 days and immunostained for BrdUrd after a 2 hour pulse with 100 μmol/L BrdUrd. **F,** The percentage of BrdUrd$^+$ cells among control (DMSO) or Shh-treated MB cells was quantified. **G–N,** MB cells cultured alone (**G** and **H**) or co-cultured with TAA (**I** and **J**) together with 1% 5E1 (**K** and **L**) were immunostained for Ki67, Zic1, or GFP. MB cells were treated with NB-B27 (control), TAA-CM, or together with 5E1 for 48 hours and immunostained for Ki67 (**N**). The percentage of Ki67$^+$ cells among cultured MB cells was quantified in **M** and **N**. **O–S**, MB slices were immunostained for Ki67 after being culture without treatment (**O** and **P**) or 5E1 (**Q** and **R**) for 4 days. The percentage of Ki67$^+$ cells among MB cells in MB slices was quantified (**S**). DAPI was used to counterstain cell nuclei in **C**, **E**, **O**, and **Q**. Data in **A**, **F**, **M**, **N,** and **S** represent means ± SEM from three independent experiments. Scale bar, 10 μm.

above data demonstrate that TAA efficiently export functional Shh into the MB microenvironment.

TAA-derived Shh supports MB cell proliferation

We next investigated the possible contribution of Shh to MB cell proliferation in the tumor microenvironment. MB cells from *Math1-Cre/Ptch1$^{fl/fl}$* mice were cultured *in vitro* and cells were examined at different time points to determine the level of proliferation. As shown in Fig. 3A, a majority of MB cells were proliferating after 24 hours in culture. However, MB cells started exiting the cell cycle after 48 hours in culture, with only 10% still dividing at 96 hours. These data suggest that MB cells gradually cease proliferation *in vitro*. The expression of Gli1 also progressively declined in cultured MB cells during the same time frame

(Supplementary Fig. S2A), indicating that hedgehog pathway activity is rapidly downregulated when MB cells are cultured *in vitro*, as shown previously (35). To examine whether exogenous Shh can support tumor cell proliferation *in vitro*, MB cells were cultured in the presence of 1 μg/mL recombinant Shh. As shown in Fig. 3B–F, approximately 15% of MB cells were BrdUrd positive after 72 hours in the control culture. However, almost 30% of MB cells were BrdUrd positive when cultured in the presence of Shh, indicating that exogenous Shh enhances MB cell proliferation *in vitro*.

To examine whether TAA promote MB cell proliferation by secreting Shh, we treated cocultures of TAA and MB cells with the Shh-neutralizing antibody 5E1 (36). As a control, we treated cerebellar GNPs with Shh in the presence and absence of 5E1. As shown in Supplementary Fig. S2B, 5E1 significantly repressed upregulation of *Gli1* and *cyclin D1* in GNPs following Shh treatment, indicating that 5E1 is capable of antagonizing Shh. MB cells and TAA were isolated from *Math1-Cre/Ptch1$^{fl/fl}$/GFAP-GFP* mice at 8 weeks of age, then the purified MB cells were cultured alone, or with TAA, in the presence and absence of 5E1. At 48 hours after treatment, cells were examined by immunostaining with Ki67 and Zic1 antibodies (Fig. 3G and H). When cultured alone, approximately 40% of MB cells were proliferative (Ki67$^+$) and no alterations in MB cell proliferation were found after treatment with 5E1. However, MB cell proliferation was dramatically enhanced in the presence of TAA (Fig. 3I and J). TAA-enhanced proliferation of MB cells was significantly inhibited by 5E1 treatment (Fig. 3K–M), suggesting that TAA stimulated MB cell proliferation through Shh secretion. There still remains a possibility that Shh could stimulate proliferation of MB cells through upregulation of other factors in astrocytes. To address this, we cultured TAA for 48 hours before collecting conditioned medium (TAA-CM). MB cells were treated with NB-B27 (control), TAA-CM [NB-B27 + TAA-CM (1:1)], or TAA-CM + 5E1. Forty-eight hours after treatment, MB cells were harvested for immunocytochemistry with an antibody against Ki67. TAA-CM dramatically increased MB cell proliferation, compared with NB-B27. Enhanced proliferation of MB cells in the presence of TAA-CM, was effectively repressed by 5E1 (Fig. 3N). These data indicate that Shh from TAA directly stimulate MB cell proliferation.

To further investigate the supporting role of Shh in the tumor microenvironment, we used organotypic slice cultures (24), to examine the blocking activity of 5E1. Tumor slices were prepared from MB developed in *Math1-Cre/Ptch1$^{fl/fl}$* mice at 8 weeks of age as previously described (24), and treated without and with 5E1 for 4 days. Following treatment, tumor slices were examined by IHC to determine the effects of Shh abrogation on proliferation. As shown in Fig. 3O and P, there was robust proliferation of MB cells in the tumor slices, with 40% of MB cells positive for Ki67 after 4 days. The level of proliferation was significantly elevated in tumor slices compared with cell culture, highlighting the important role of the tumor microenvironment in MB cell proliferation. This enhanced level of MB cells proliferation was reduced to 12% by 5E1 treatment of the tumor slices (Fig. 3Q–S). No increase in apoptosis or cell death was observed in tumor slices after 5E1 treatment (Supplementary Fig. S3A–S3C). These data demonstrate that Shh, present in the tumor microenvironment, is required for MB cell proliferation.

Shh induces Nestin expression in *Ptch1*-deficient GNPs

Recently, we reported that Nestin expression level increase during tumor progression and that it plays a key role in enhancing Hedgehog pathway activity and MB cell proliferation *in vivo* (22). Having observed that Shh can promote MB cell proliferation, we examined whether Shh affects Nestin expression in MB cells. For this purpose, we utilized *Math1-Cre/Ptch1$^{fl/fl}$/Nestin-CFP* mice, in which MB cells gradually increase the levels of Nestin, presented by cyan fluorescent protein (CFP) expression as tumors develop (22). Nestin-negative (CFP$^-$) cells were purified by FACS from *Math1-Cre/Ptch1$^{fl/fl}$/Nestin-CFP* mice at P7. At this age, only 20% of *Ptch1*-deficient GNPs express Nestin (CFP$^+$) in the cerebellum (22). *Ptch1* deletion, as well as activation of the hedgehog pathway in CFP$^-$ cells, was previously demonstrated by qPCR and Western blot analyses (22). CFP$^-$ cells were treated with recombinant Shh alone or together with 5E1. After 48 hours culture, only a few Nestin-expressing cells were present in the cultures based on immunocytochemistry (Fig. 4A and B). However, Shh treatment significantly increased Nestin expression among *Ptch1*-deficient GNPs (Fig. 4C and D). Moreover, Shh-induced Nestin expression was effectively blocked by 5E1 (Fig. 4E and F). On the basis of qRT-PCR analysis, Shh significantly enhanced the level of Nestin mRNA expression in *Ptch1*-deficient GNPs, whereas Shh-induced Nestin expression was markedly reduced following 5E1 treatment (Fig. 4G). No alteration in the expression of *Nestin* or *Gli1* mRNA was observed in *Ptch1*-deficient GNPs after treatment with 5E1 alone (Fig. 4G). These data reveal that Shh is capable of inducing *Nestin* mRNA expression in *Ptch1*-deficient GNPs.

To investigate whether astrocytes can stimulate Nestin expression in *Ptch1*-deficient GNPs through Shh secretion, we purified CFP$^-$ GNPs as mentioned above, and isolated TAA from *Math1-Cre/Ptch1$^{fl/fl}$/GFAP-GFP* mice. CFP$^-$ GNPs were cultured alone, or with TAA, at a ratio (MB cells to TAA) of 5:1 in the presence and absence of 5E1 for 48 hours. We then examined Nestin induction in *Ptch1*-deficient GNPs using CFP expression as a marker. As shown in Fig. 4H, spontaneous CFP$^+$ cells were identified at a low level in *Ptch1*-deficient GNPs cultured alone. This low-level spontaneous expression was not dependent on exogenous Shh, as 5E1 treatment had no effect on CFP expression (Fig. 4I). In the presence of TAA that already extended elongated processes (Fig. 4J), the number of CFP$^+$ cells dramatically increased in the *Ptch1*-deficient GNP population (Fig. 4K). Treatment of these cocultures with 5E1 suppressed the number of CFP$^+$ cells (Fig. 4L–N). These data indicate that TAA-induced Nestin expression in *Ptch1*-deficient GNPs is mediated by Shh secretion.

Shh-induced Nestin expression relies on Smo activation, but is independent of Gli1

Shh-induced Nestin expression in *Ptch1*-deficient GNPs reveals a distinct function of Shh that is independent of binding to Ptch1. To further characterize the mechanism involved in Shh-induced Nestin expression, we isolated CFP$^-$, *Ptch1*-deficient GNPs from *Math1-Cre/Ptch1$^{fl/fl}$/Nestin-GFP* mice and treated them with 1 μg/mL recombinant Shh, in the presence and absence of cyclopamine, a potent naturally occurring plant alkaloid that antagonizes Smo (37). As shown in Fig. 5A and B, nearly no Nestin expression was detected in *Ptch1*-deficient GNPs at control conditions. In contrast, approximately 22% of *Ptch1*-deficient GNPs exhibited Nestin expression after Shh treatment (Fig. 5C and D). However, cyclopamine dramatically blocked the increase

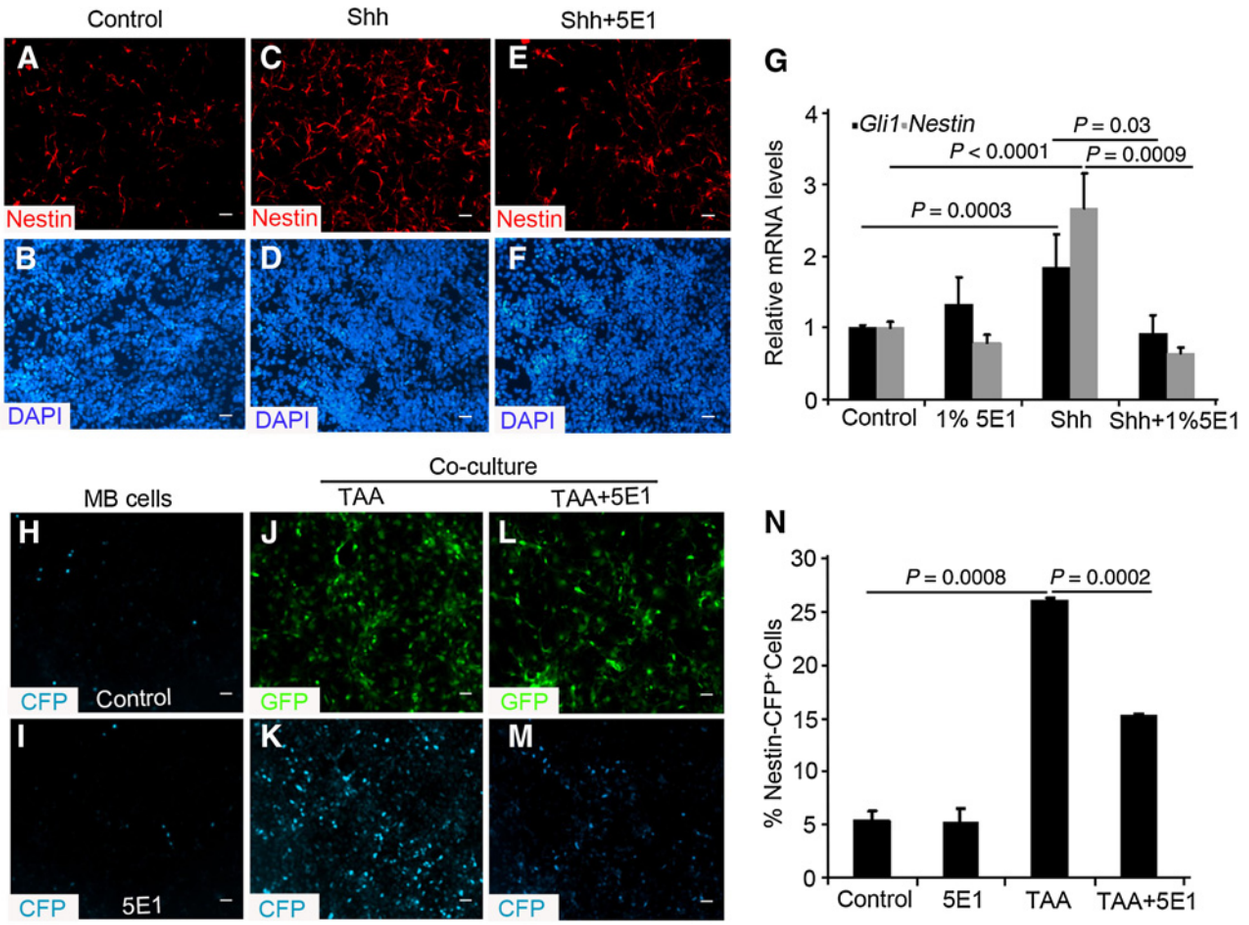

Figure 4.

TAA-derived Shh induces Nestin expression in MB cells. **A–F,** CFP-negative *Ptch1*-deficient GNPs from *Math1-Cre/Ptch1*$^{fl/fl}$*/Nestin-CFP* mice at P7 were immunostained with Nestin after treatment with PBS control (**A** and **B**), 1 μg/mL Shh (**C** and **D**), or Shh plus 1% 5E1 (**E** and **F**) for 48 hours. **G,** Expression of *Gli1* and *Nestin* mRNA in CFP-negative *Ptch1*-deficient GNPs treated with 1% 5E1, 1 μg/mL Shh, or Shh plus 5E1 for 48 hours was examined by qPCR. **H–M,** CFP-negative *Ptch1*-deficient GNPs were cultured alone (**H** and **I**) or cocultured with TAA (GFP$^+$, **J–M**) in the absence and presence of 5E1. **N,** The percentage of Nestin-CFP$^+$ cells among *Ptch1*-deficient GNPs was quantified. Data in **G** and **N** represent means ± SEM from three independent experiments. Scale bar, 10 μm.

in Nestin mRNA and protein in *Ptch1*-deficient GNPs following Shh treatment (Fig. 5E–G), indicating that Smo activation is required for Shh-induced Nestin expression.

We next investigated whether Shh-induced Nestin expression is mediated by *Gli1*. Cerebellar GNPs isolated from p8 wild-type mice were infected with a lentiviral vector expressing HA-tagged *Gli1*. Approximately, 48 hours after infection, cultured GNPs were harvested for immunocytochemistry and qRT-PCR analysis. As shown in Fig. 5H and I, no Nestin was detected in *Gli1*-infected GNPs, regardless of the presence of Shh (Fig. 5J and K). In contrast, it was clear that exogenous *Gli1* induced expression of *cyclin D1*, a Shh pathway target gene (Fig. 5L; ref. 33). Nevertheless, no induction of Nestin mRNA was detected in GNPs after *Gli1* overexpression and Shh treatment (Fig. 5L). In addition, Nestin negative cells purified from *Math1-Cre/Ptch1*$^{fl/fl}$*/Nestin-CFP* mice at P7 were infected with a lentivirus carrying a HA-tagged Gli1 vector or a HA-tagged empty vector. Forty-eight hours after infection, no Nestin expression was observed in Gli1-overexpressed or the control cells (Supplementary Fig. S4A–S4D). These data suggest that Gli1 is not sufficient for Shh-induced Nestin expression in cerebellar GNPs.

Taken together, the above data indicate that, although Shh-induced Nestin expression in *Ptch1*-deficient GNPs requires Smo activation, it is independent of Gli1.

TAAs are required for MB progression

To investigate the role of TAA in MB progression, we examined MB growth after ablation of TAA in *GFAP-TK* mice. In these mice, astrocytes express thymidine kinase (TK), which renders them sensitive to ganciclovir (GCV) treatment (38). *GFAP-TK* mice were crossed with *Math1-Cre/Ptch1*$^{fl/fl}$ mice. As shown in Fig. 6A–C, more than 95% of TAA (S100β$^+$) were positive for TK, indicating that *Math1-Cre/Ptch1*$^{fl/fl}$*/GFAP-TK* mice could be used to target TAA by GCV treatment (100 mg/kg). We treated *Math1-Cre/Ptch1*$^{fl/fl}$*/GFAP-TK* mice at 8 weeks of age with GCV or saline vehicle control once daily for 7 days. Before and after GCV treatment, tumor volume was examined by MRI. As shown in Fig. 6D and E, the tumor volume decreased dramatically in

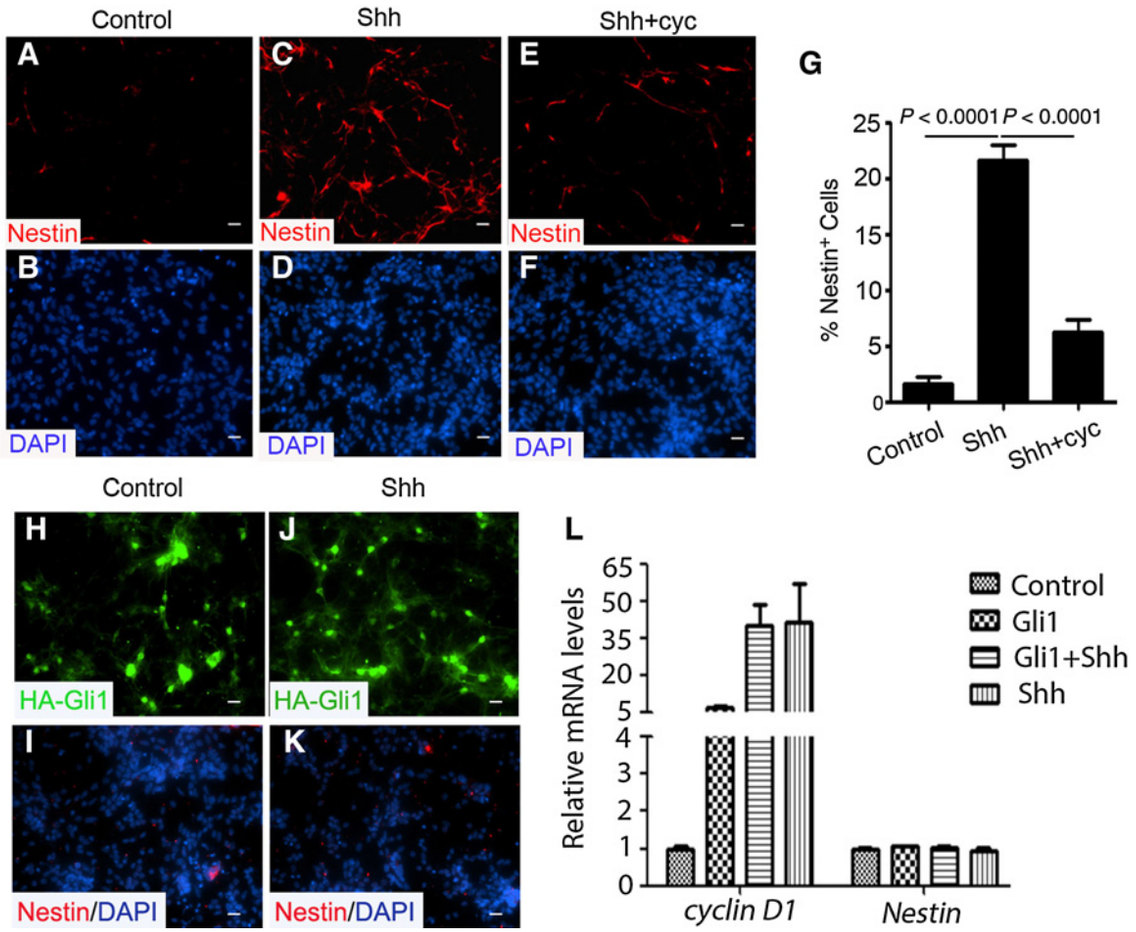

Figure 5.

Shh-induced Nestin expression requires Smo but not Gli1. **A–F,** CFP-negative *Ptch1*-deficient GNPs from *Math1-Cre/Ptch1*$^{fl/fl}$*/Nestin-CFP* mice at P7 were immunostained with Nestin after treatment with PBS (**A** and **B**), 1 μg/mL Shh (**C** and **D**), or Shh plus 1 μmol/L cyclopamine (cyc; **E** and **F**) for 48 hours. **G,** The percentage of Nestin$^+$ cells among *Ptch1*-deficient GNPs treated with PBS control, Shh, and Shh plus cyc was quantified. **E–H,** wild-type GNPs infected with a lentivirus carrying HA-Gli1 were treated without (**H** and **I**) or with Shh (**J** and **K**) for 2 days and immunostained for HA or Nestin. **I,** Expressions of *cyclin D1* and *Nestin* mRNAs in infected GNPs were examined by qRT-PCR. The values in **G** and **L** are the means ± SEM from three independent experiments. Scale bar, 10 μm.

Math1-Cre/Ptch1$^{fl/fl}$*/GFAP-TK* mice following GCV treatment, compared with that prior to GCV treatment (Fig. 6F). These data demonstrate that ablation of TAA significantly suppresses MB growth *in vivo*.

To determine the basis for inhibition of MB growth after deletion of TAA, we crossed *Math1-Cre/Ptch1*$^{fl/fl}$*/GFAP-TK* mice with *Nestin-CFP* mice, then examined MB cells proliferation and Nestin expression in MB cells. *Math1-Cre/Ptch1*$^{fl/fl}$*/GFAP-TK/Nestin-CFP* mice were treated with GCV or saline by subcutaneous injection. Robust CFP expression was observed in tumors arising in *Math1-Cre/Ptch1*$^{fl/fl}$*/GFAP-TK/Nestin-CFP* mice after saline treatment as expected (Fig. 6G). However, the level of CFP expression in MB tissue was dramatically decreased following GCV treatment (Fig. 6G), suggesting that ablation of TAA significantly reduced Nestin expression in MB tissue. Next, frozen sagittal frozen sagittal were prepared from MB obtained from *Math1-Cre/Ptch1*$^{fl/fl}$*/GFAP-TK/Nestin-CFP* mice after the above treatment, to examine CFP expression and proliferation by immnuohistochemistry. As shown in Supplementary Fig. S5A and S5B, the number of TK-positive cells was significantly decreased after GCV treatment, compared with controls, suggesting that GCV treatment effectively ablated TAA from tumor tissue. Very few CFP-expressing cells remained in tumor tissue after GCV treatment. In contrast, more than 95% of MB cells were positive for CFP (Fig. 6H and I) in mice treated with saline. Moreover, a significant reduction in the number of Ki67$^+$ cells was found in GCV-treated MB tissue compared with the control (Fig. 6J and K), suggesting that MB cell proliferation was dramatically compromised by GCV treatment. No obvious increase in apoptosis was detected in GCV-treated MB tissue (Supplementary Fig. S5C and S5D), suggesting that the survival of MB cells was not affected by GCV treatment. Interestingly, increased differentiation (NeuN$^+$) was observed in MB tissue after GCV treatment, whereas only a few differentiating MB cells were apparent in tumor tissue after saline treatment (Fig. 6L–N). These data indicate that ablation of TAA significantly inhibits tumor growth by blocking tumor cell proliferation while promoting differentiation. This is consistent with our previous finding regarding the functions of Nestin in MB tumorigenesis

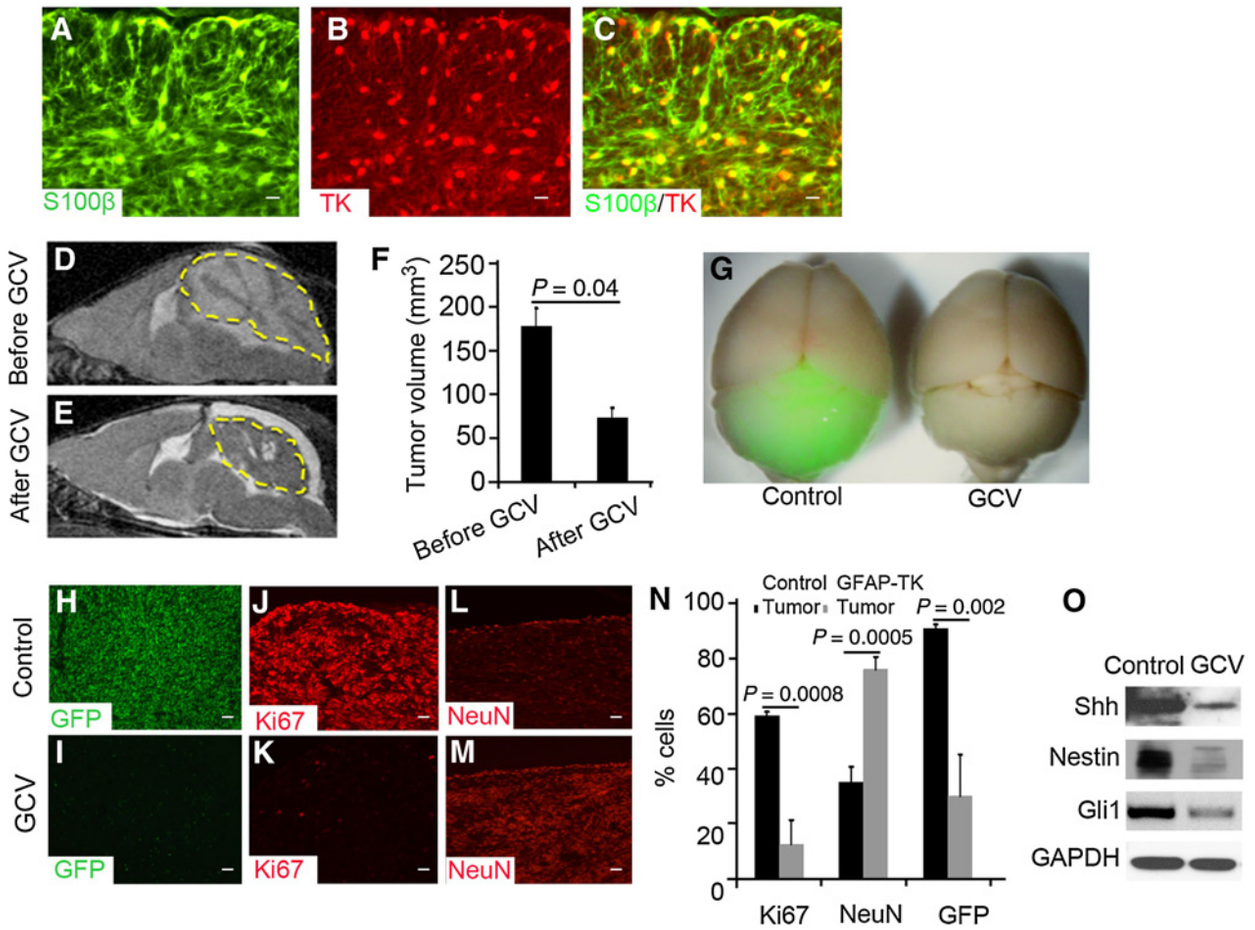

Figure 6.

TAAs are required for MB progression. **A–C,** Sagittal sections from *Math1-Cre/Ptch1$^{fl/fl}$/GFAP-TK* mice at 8 weeks of age were immunostained for S100β (**A**) and TK (**B**). A merged image (**C**) shows TK-positive cells expressed S100β. **D** and **E,** Tumor volume of MB from a *Math1-Cre/Ptch1$^{fl/fl}$/GFAP-TK* mouse before (**D**) and after (**E**) treatment with GCV for 7 days was measured by MRI. The yellow dotted lines circle the tumor mass. **F,** MB tumor volume was quantified based on MRI images using Image J software. **G,** Whole mount brain images of *Math1-Cre/Ptch1$^{fl/fl}$/GFAP-TK/Nestin-CFP* mice treated with saline (control) or GCV for 7 days. **H–M,** Sagittal sections of MB tissues from *Math1-Cre/Ptch1$^{fl/fl}$/Nestin-CFP/GFAP-TK* mice following treatment with saline (**H**, **J**, and **L**) or GCV (**I**, **K**, and **M**) for 3 days were immunostained for CFP (**H** and **I**), Ki67 (**J** and **K**), or NeuN (**L** and **M**). **N,** The percentage of Ki67, NeuN, or Nestin-CFP–positive cells in MB tissues after treatment with saline or GCV was quantified. **O,** Expression of Nestin, Gli1, Shh, or GAPDH proteins in *Math1-Cre/Ptch1$^{fl/fl}$/Nestin-CFP/GFAP-TK* MB tissue treated with saline or GCV for 3 days was examined by Western blotting. Data in **F** and **N** represent mean ± SEM from three independent experiments. Scale bar, 10 μm.

(22). After GCV or saline treatment, tumor tissue was harvested to determine the level of expression of Shh, Nestin and Gli1 by Western analyses (Fig. 6O). The amount of Shh in MB tissue significantly declined following GCV treatment, which supports the hypothesis that Shh in MB tissue is predominately derived from TAA. The levels of Nestin and Gli1 also decreased dramatically after GCV treatment, consistent with our finding that TAA-derived Shh enhances activation of the hedgehog pathway in MB cells by induction of Nestin expression. These data demonstrate that TAA support MB cell proliferation and tumor growth by secretion of Shh.

Discussion

Solid tumors are no longer viewed as monoclonal collections of cancer cells. Instead, they are best described as multicellular organs harboring diverse, dynamic populations of neoplastic as well as normal cells (39). The relative proportions of the various cell populations change during tumor progression and over the course of therapy. Understanding the relationships among different cell types in the tumor microenvironment is key to understanding the biology of tumor initiation, progression, and metastasis. It also has the potential to provide additional avenues for therapeutic intervention. The tumor microenvironment not only contributes to neoplastic growth, it also regulates responses to chemotherapy and radiotherapy (40). Although the molecular mechanisms underlying tumorigenesis of hedgehog pathway in MB has been studied extensively, the contributions of the tumor microenvironment to MB initiation and progression remain elusive. Here we demonstrate that astrocytes, a major cellular component of the MB microenvironment, promote tumor progression through Shh secretion. Ablation of astrocytes markedly

prohibited MB growth by reducing proliferation of MB cells. These findings, for the first time, reveal an indispensable role for astrocytes in hedgehog-type MB, which highlight the importance of the tumor microenvironment in tumor progression.

Our previous studies revealed that, following *Ptch1* loss, GNPs progressively express Nestin as an obligatory step in MB development (22). However, the mechanism responsible for increased Nestin expression in *Ptch1*-deficient GNPs was not known. Here, we demonstrate that astrocyte-derived Shh is responsible for induction of Nestin expression in *Ptch1*-deficient GNPs and MB cells. In the canonical hedgehog pathway, Shh binds to Ptch1, resulting in release of Smo that, in turn, inhibits Sufu, leading to activation of Gli1 and Gli2 and regulation of target gene expression. However, this does not appear to be the underlying mechanism whereby Shh induces Nestin expression in *Ptch1*-deficient GNPs. Neither deletion of *Ptch1* nor overexpression of *Gli1* was sufficient to stimulate Nestin expression in cerebellar GNPs. Nestin was only expressed in *Ptch1*-deficient GNPs after Shh treatment. This paradoxical effect of Shh in the absence of its receptor Ptch1 implies a role for additional Shh receptors such as Ptch2 or Boc. In particular, Ptch2 has been reported to mediate the response of fibroblasts to Shh in the absence of Ptch1 (41). Moreover, Ptch2 modulates MB tumorigenesis in mice with *Ptch1* haploinsufficiency (42). Although we attempted to examine the possible involvement of Ptch2 or Boc in Shh-induced Nestin expression, we failed to effectively knockdown these two genes in MB cells using shRNA or siRNA, which is likely due to substantially increased expression of *Ptch2* and *Boc* in MB cells (data not shown). Nevertheless, because cyclopamine blocked Shh-induced Nestin expression in *Ptch1*-deficient GNPs, activated Smo is still further required for this novel function of Shh. Nestin does not appear to be a classic Hh pathway target gene because it was not induced by overexpression of *Gli1*. These data indicate that Shh stimulates Nestin expression in GNPs and MB cells in a Smo-dependent, but Gli1-independent manner. Previously, we demonstrated that Nestin augments canonical Shh signaling by abolishing the inhibitory functions of Gli3 (22). Taken together, our findings reveal a novel, paradoxical signaling pathway in which Shh, Smo, and Nestin, acting in concert, regulate hedgehog pathway activity in normal and neoplastic cells, independently of Ptch1 and Gli1.

During cerebellar development, the Shh pathway drives a massive expansion of cerebellar GNPs (33). However, Shh-induced Nestin expression was found only in *Ptch1*-deficient GNPs but not in wild-type GNPs (Fig. 5H–L). One possible explanation for this observation is that the extent of Smo activation may dictate whether Nestin expression can be induced by Shh in GNPs. As the predominant antagonizing partner of Smo, *Ptch1* is also a target gene of hedgehog pathway activity. In wild-type GNPs, Shh treatment also increases *Ptch1* expression, subsequently restricting the activation of Smo. However, the negative feedback loop, mediated by *Ptch1*, is disrupted in *Ptch1*-deficient GNPs and in MB cells, resulting in overactivation of Smo. Future studies are warranted to further investigate the molecular events downstream of Smo that mediate Shh-induced Nestin expression in MB cells.

Previously, we reported that MB cells cannot maintain an active Shh pathway *in vitro*. However, if tumor tissue was never cultured but directly implanted in a flank allograft, the Shh pathway remains active in MB cells (35). Here, we provide an explanation for this conundrum. The addition of exogenous Shh, or coculture with TAA, significantly augmented Shh pathway activity in cultured MB cells, resulting in continued proliferation *in vitro*. These findings indicate that astrocyte-derived Shh, secreted into the tumor microenvironment, is required for maintaining an active hedgehog pathway in MB cells. This support from the tumor microenvironment is lost when MB cells are cultured *in vitro*. In the case of allograft transplantation, host stromal cells may invade and rebuild the tumor microenvironment to maintain an active Shh pathway in MB cells. Several groups, including our own, have made many unsuccessful attempts to establish PDX models for Shh type MB. Only approximately 10% of human MB samples can be propagated in immunosuppressed mice, and the tumors that grow fail to maintain an active hedgehog pathway (data not shown). Our findings suggest an alternative approach, in which stromal cells, including astrocytes, could be coinjected with MB cells in an attempt to recreate the tumor microenvironment and provide support to enhance the survival and propagation of human MB cells after grafting into immunosuppressed mice. In addition, based on our studies, exogenous Shh may be required in the culture media to maintain hedgehog pathway activity in MB cells *in vitro*.

In our studies, tumor volume in *Math1-Cre/Ptch1$^{fl/fl}$/GFAP-TK/Nestin-CFP* mice was dramatically decreased after GCV treatment, raising the possibility that the reduction in tumor size may be due to the "bystander effect." The "bystander effect" is well documented in tumor models (43, 44), in which cells in the vicinity of TK-expressing cells are killed by GCV. It was attributed to the transfer of phosphorylated GCV from cell to cell through gap junction (45). However, no gap junctions between astrocytes and GNPs (MB cells) were found based on previous studies of cerebellar architecture (46). In addition, the previously reported "bystander effect" is associated with a significant amount of cell death, and the effect itself is to increase cell death. For example, more than 90% of cell death was detected in tumor tissues carrying the TK gene after GCV treatment (43, 44). However, no increase in cell death within the tumor tissue was found following GCV treatment in our studies (Supplementary Fig. S4). The predominant effect of GCV treatment in *Math1-Cre/Ptch1$^{fl/fl}$/GFAP-TK/Nestin-CFP* mice was induction of tumor cell differentiation and repression of Nestin expression in MB cells. Although we cannot completely rule out the "bystander effect," we believe that the "bystander effect" is not the reason for reduced tumor volume observed in *Math1-Cre/Ptch1$^{fl/fl}$/GFAP-TK/Nestin-CFP* mice after GCV treatment.

The Smo inhibitors, vismodegib and sonidegib, are currently approved for the treatment of advanced basal cell carcinoma (BCC) and they have demonstrated efficacy in clinical trials of Hh-MB (47–49). Despite the dramatic response to these inhibitors in the initial clinical trials, drug resistance readily arises in both human and animal models as a consequence of mutation in Smo (50), amplification of Gli2 (51), or cyclin D1 (52). Because of significant toxicities, many BCC patients cannot endure prolonged therapy and often come off drug only to go back on when tumors recur (53). In children, there is a greater concern for developmental toxicities as the Hh pathway is primarily active during development. Transient treatment of young mice with a Smo antagonist caused dramatic and permanent defects in bone development (54). These observations are consistent with the critical functions that the hedgehog pathway plays in bone growth (55). Recently, similar effects were seen in children and the FDA required modifications of

the protocol excluding children in which bone growth is active unless there are no other treatment options. Here we demonstrate a major role for astrocyte-derived Shh in activation of the Shh pathway in MB cells through induction of Nestin expression. This effect was only observed in *Ptch1*-deficient GNPs and MB cells, but not in wild-type GNPs. This suggests that targeting astrocytes, or the secretion of Shh, may represent tumor-specific strategies for therapeutic intervention in MB and other Hh pathway malignancies, such as BCC.

Disclosure of Potential Conflicts of Interest

No potential conflicts of interest were disclosed.

Authors' Contributions

Conception and design: L.W. Yuelling, J.M.Y. Ng, H. Liu, T. Curran, Z.-J. Yang
Development of methodology: L.W. Yuelling, F. Du, J.M.Y. Ng, S. Robins, Z.-J. Yang
Acquisition of data (provided animals, acquired and managed patients, provided facilities, etc.): Y. Liu, L.W. Yuelling, F. Du, R.E. Gordon, J.A. O'Brien, J.M.Y. Ng, Z.-J. Yang
Analysis and interpretation of data (e.g., statistical analysis, biostatistics, computational analysis): Y. Liu, L.W. Yuelling, Y. Wang, J.M.Y. Ng, H. Liu, T. Curran, Z.-J. Yang
Writing, review, and/or revision of the manuscript: Y. Liu, L.W. Yuelling, Y. Wang, J.M.Y. Ng, H. Liu, T. Curran, Z.-J. Yang
Administrative, technical, or material support (i.e., reporting or organizing data, constructing databases): L.W. Yuelling, F. Du, J.M.Y. Ng, E.H. Lee, Z.-J. Yang
Study supervision: J.M.Y. Ng, Z.-J. Yang

Acknowledgments

We thank J. Oesterling for flow cytometric analysis; E. Nicholas for qPCR analysis; and Dr. R. Segal (Dana Farber Cancer Institute) for anti-Zic1 antibody; Dr. M. Sofroniew (University of California, Los Angeles) for anti-TK antibody.

Grant Support

This research was supported by funds from the U.S. National Cancer Institute (CA178380 and CA185504 to Z. Yang; T32 CA009035-45, to L.W. Yuelling), American Cancer Society (RSG1605301NEC to Z. Yang), Pennsylvania Department of Health (CURE 4100068716 to Z. Yang), and National Natural Science Foundation of China (81572724 to Z. Yang).

The costs of publication of this article were defrayed in part by the payment of page charges. This article must therefore be hereby marked *advertisement* in accordance with 18 U.S.C. Section 1734 solely to indicate this fact.

Received June 13, 2017; revised August 10, 2017; accepted September 26, 2017; published OnlineFirst October 6, 2017.

References

1. Barres BA. The mystery and magic of glia: a perspective on their roles in health and disease. Neuron 2008;60:430–40.
2. Nedergaard M, Ransom B, Goldman SA. New roles for astrocytes: redefining the functional architecture of the brain. Trends Neurosci 2003;26:523–30.
3. Hol EM, Pekny M. Glial fibrillary acidic protein (GFAP) and the astrocyte intermediate filament system in diseases of the central nervous system. Curr Opin Cell Biol 2015;32:121–30.
4. Ghandour MS, Labourdette G, Vincendon G, Gombos G. A biochemical and immunohistological study of S100 protein in developing rat cerebellum. Dev Neurosci 1981;4:98–109.
5. Sharma K, Schmitt S, Bergner CG, Tyanova S, Kannaiyan N, Manrique-Hoyos N, et al. Cell type- and brain region-resolved mouse brain proteome. Nat Neurosci 2015;18:1819–31.
6. Kurtz A, Zimmer A, Schnutgen F, Bruning G, Spener F, Muller T. The expression pattern of a novel gene encoding brain-fatty acid binding protein correlates with neuronal and glial cell development. Development 1994;120:2637–49.
7. De Zeeuw CI, Hoogland TM. Reappraisal of Bergmann glial cells as modulators of cerebellar circuit function. Front Cell Neurosci 2015;9:246. doi: 10.3389/fncel.2015.00246.
8. Myer DJ, Gurkoff GG, Lee SM, Hovda DA, Sofroniew MV. Essential protective roles of reactive astrocytes in traumatic brain injury. Brain 2006;129(Pt 10):2761–72.
9. Seifert G, Schilling K, Steinhauser C. Astrocyte dysfunction in neurological disorders: a molecular perspective. Nat Rev Neurosci 2006;7:194–206.
10. Kim SJ, Kim JS, Park ES, Lee JS, Lin Q, Langley RR, et al. Astrocytes upregulate survival genes in tumor cells and induce protection from chemotherapy. Neoplasia 2011;13:286–98.
11. Thompson MC, Fuller C, Hogg TL, Dalton J, Finkelstein D, Lau CC, et al. Genomics identifies medulloblastoma subgroups that are enriched for specific genetic alterations. J Clin Oncol 2006;24:1924–31.
12. Kool M, Korshunov A, Remke M, Jones DT, Schlanstein M, Northcott PA, et al. Molecular subgroups of medulloblastoma: an international meta-analysis of transcriptome, genetic aberrations, and clinical data of WNT, SHH, Group 3, and Group 4 medulloblastomas. Acta Neuropathol 2012;123:473–84.
13. Northcott PA, Nakahara Y, Wu X, Feuk L, Ellison DW, Croul S, et al. Multiple recurrent genetic events converge on control of histone lysine methylation in medulloblastoma. Nat Genet 2009;41:465–72.
14. Varjosalo M, Taipale J. Hedgehog: functions and mechanisms. Genes Dev 2008;22:2454–72.
15. Humke EW, Dorn KV, Milenkovic L, Scott MP, Rohatgi R. The output of Hedgehog signaling is controlled by the dynamic association between Suppressor of Fused and the Gli proteins. Genes Dev 2010;24:670–82.
16. Aza-Blanc P, Ramirez-Weber FA, Laget MP, Schwartz C, Kornberg TB. Proteolysis that is inhibited by hedgehog targets Cubitus interruptus protein to the nucleus and converts it to a repressor. Cell 1997;89:1043–53.
17. Jenkins D. Hedgehog signalling: emerging evidence for non-canonical pathways. Cell Signal 2009;21:1023–34.
18. Chinchilla P, Xiao L, Kazanietz MG, Riobo NA. Hedgehog proteins activate pro-angiogenic responses in endothelial cells through non-canonical signaling pathways. Cell Cycle 2010;9:570–9.
19. Bijlsma MF, Borensztajn KS, Roelink H, Peppelenbosch MP, Spek CA. Sonic hedgehog induces transcription-independent cytoskeletal rearrangement and migration regulated by arachidonate metabolites. Cell Signal 2007;19:2596–604.
20. Yam PT, Langlois SD, Morin S, Charron F. Sonic hedgehog guides axons through a noncanonical, Src-family-kinase-dependent signaling pathway. Neuron 2009;62:349–62.
21. Yang ZJ, Ellis T, Markant SL, Read TA, Kessler JD, Bourboulas M, et al. Medulloblastoma can be initiated by deletion of Patched in lineage-restricted progenitors or stem cells. Cancer Cell 2008;14:135–45.
22. Li P, Lee E, Du F, Gordon RE, Yuelling LW, Liu Y, et al. Nestin mediates hedgehog pathway tumorigenesis. Cancer Res 2016;76:5573–83.
23. Li P, Du F, Yuelling LW, Lin T, Muradimova RE, Tricarico R, et al. A population of Nestin-expressing progenitors in the cerebellum exhibits increased tumorigenicity. Nat Neurosci 2013;16:1737–44.
24. Chadwick EJ, Yang DP, Filbin MG, Mazzola E, Sun Y, Behar O, et al. A brain tumor/organotypic slice co-culture system for studying tumor microenvironment and targeted drug therapies. J Vis Exp 2015;105:e53304.
25. Gajjar AJ, Robinson GW. Medulloblastoma-translating discoveries from the bench to the bedside. Nat Rev Clin Oncol 2014;11:714–22.
26. Northcott PA, Korshunov A, Witt H, Hielscher T, Eberhart CG, Mack S, et al. Medulloblastoma comprises four distinct molecular variants. J Clin Oncol 2011;29:1408–14.
27. Yokota N, Aruga J, Takai S, Yamada K, Hamazaki M, Iwase T, et al. Predominant expression of human zic in cerebellar granule cell lineage and medulloblastoma. Cancer Res 1996;56:377–83.
28. Goodrich LV, Milenkovic L, Higgins KM, Scott MP. Altered neural cell fates and medulloblastoma in mouse patched mutants. Science 1997;277:1109–13.

29. Schuller U, Heine VM, Mao J, Kho AT, Dillon AK, Han YG, et al. Acquisition of granule neuron precursor identity is a critical determinant of progenitor cell competence to form Shh-induced medulloblastoma. Cancer Cell 2008;14:123–34.
30. Zhuo L, Sun B, Zhang CL, Fine A, Chiu SY, Messing A. Live astrocytes visualized by green fluorescent protein in transgenic mice. Dev Biol 1997;187:36–42.
31. Barry D, McDermott K. Differentiation of radial glia from radial precursor cells and transformation into astrocytes in the developing rat spinal cord. Glia 2005;50:187–97.
32. Alvarez JI, Dodelet-Devillers A, Kebir H, Ifergan I, Fabre PJ, Terouz S, et al. The Hedgehog pathway promotes blood-brain barrier integrity and CNS immune quiescence. Science 2011;334:1727–31.
33. Wechsler-Reya RJ, Scott MP. Control of neuronal precursor proliferation in the cerebellum by Sonic Hedgehog. Neuron 1999;22: 103–14.
34. Taipale J, Chen JK, Cooper MK, Wang B, Mann RK, Milenkovic L, et al. Effects of oncogenic mutations in Smoothened and Patched can be reversed by cyclopamine. Nature 2000;406:1005–9.
35. Sasai K, Romer JT, Lee Y, Finkelstein D, Fuller C, McKinnon PJ, et al. Shh pathway activity is down-regulated in cultured medulloblastoma cells: implications for preclinical studies. Cancer Res 2006;66:4215–22.
36. Ericson J, Morton S, Kawakami A, Roelink H, Jessell TM. Two critical periods of Sonic Hedgehog signaling required for the specification of motor neuron identity. Cell 1996;87:661–73.
37. Chen JK, Taipale J, Cooper MK, Beachy PA. Inhibition of Hedgehog signaling by direct binding of cyclopamine to Smoothened. Genes Dev 2002;16:2743–8.
38. Delaney CL, Brenner M, Messing A. Conditional ablation of cerebellar astrocytes in postnatal transgenic mice. J Neurosci 1996;16:6908–18.
39. Egeblad M, Nakasone ES, Werb Z. Tumors as organs: complex tissues that interface with the entire organism. Dev Cell 2010;18:884–901.
40. Polyak K, Haviv I, Campbell IG. Co-evolution of tumor cells and their microenvironment. Trends Genet 2009;25:30–8.
41. Alfaro AC, Roberts B, Kwong L, Bijlsma MF, Roelink H. Ptch2 mediates the Shh response in Ptch1-/- cells. Development 2014;141:3331–9.
42. Lee Y, Miller HL, Russell HR, Boyd K, Curran T, McKinnon PJ. Patched2 modulates tumorigenesis in patched1 heterozygous mice. Cancer Res 2006;66:6964–71.
43. Calvez V, Rixe O, Wang P, Mouawad R, Soubrane C, Ghoumari A, et al. Virus-free transfer of the herpes simplex virus thymidine kinase gene followed by ganciclovir treatment induces tumor cell death. Clin Cancer Res 1996;2:47–51.
44. Freeman SM, Abboud CN, Whartenby KA, Packman CH, Koeplin DS, Moolten FL, et al. The "bystander effect": tumor regression when a fraction of the tumor mass is genetically modified. Cancer Res 1993;53:5274–83.
45. Culver KW, Ram Z, Wallbridge S, Ishii H, Oldfield EH, Blaese RM. In vivo gene transfer with retroviral vector-producer cells for treatment of experimental brain tumors. Science 1992;256:1550–2.
46. Rakic P, Sidman RL. Organization of cerebellar cortex secondary to deficit of granule cells in weaver mutant mice. J Comp Neurol 1973;152:133–61.
47. Ng JM, Curran T. The Hedgehog's tale: developing strategies for targeting cancer. Nat Rev Cancer 2011;11:493–501.
48. Sekulic A, Migden MR, Oro AE, Dirix L, Lewis KD, Hainsworth JD, et al. Efficacy and safety of vismodegib in advanced basal-cell carcinoma. N Engl J Med 2012;366:2171–9.
49. Casey D, Demko S, Shord S, Zhao H, Chen H, He K, et al. FDA approval summary: sonidegib for locally advanced basal cell carcinoma. Clin Cancer Res 2017;23:2377–81.
50. Yauch RL, Dijkgraaf GJ, Alicke B, Januario T, Ahn CP, Holcomb T, et al. Smoothened mutation confers resistance to a Hedgehog pathway inhibitor in medulloblastoma. Science 2009;326:572–4.
51. Buonamici S, Williams J, Morrissey M, Wang A, Guo R, Vattay A, et al. Interfering with resistance to smoothened antagonists by inhibition of the PI3K pathway in medulloblastoma. Sci Transl Med 2010;2:51ra70.
52. Dijkgraaf GJ, Alicke B, Weinmann L, Januario T, West K, Modrusan Z, et al. Small molecule inhibition of GDC-0449 refractory smoothened mutants and downstream mechanisms of drug resistance. Cancer Res 2011;71:435–44.
53. Tang JY, Mackay-Wiggan JM, Aszterbaum M, Yauch RL, Lindgren J, Chang K, et al. Inhibiting the hedgehog pathway in patients with the basal-cell nevus syndrome. N Engl J Med 2012;366:2180–8.
54. Kimura H, Ng JM, Curran T. Transient inhibition of the Hedgehog pathway in young mice causes permanent defects in bone structure. Cancer Cell 2008;13:249–60.
55. St-Jacques B, Hammerschmidt M, McMahon AP. Indian hedgehog signaling regulates proliferation and differentiation of chondrocytes and is essential for bone formation. Genes Dev 1999;13:2072–86.